An X-Ray Census of Fast Radio Burst Host Galaxies

Constraints on Active Galactic Nuclei and X-Ray Counterparts

Eftekhari, T.; Fong, W.; Gordon, A.C.; Sridhar, N.; Kilpatrick, C.D.; Bhandari, S.; Deller, A.T.; Dong, Y.; Rouco Escorial, A.; Heintz, K.E.; Leja, J.; Margalit, B.; Metzger, B.D.; Pearlman, A.B.; Prochaska, J.X.; Ryder, S.D.; Scholz, P.; Shannon, R.M.; Tejos, N.

DOI
10.3847/1538-4357/acf843

Publication date
2023

Document Version
Final published version

Published in
Astrophysical Journal

The Astrophysical Journal, 958:66 (12pp), 2023 November 20 https://doi.org/10.3847/1538-4357/acf843

An X-Ray Census of Fast Radio Burst Host Galaxies: Constraints on Active Galactic Nuclei and X-Ray Counterparts

T. Eftekhari[1,26], W. Fong[1], A. C. Gordon[1], N. Sridhar[2,3], C. D. Kilpatrick[1], S. Bhandari[4,5,6,7,27], A. T. Deller[8], Y. Dong (董雨 欣)[1], A. Rouco Escorial[9,28], K. E. Heintz[10,11], J. Leja[12,13,14], B. Margalit[15], B. D. Metzger[2,3,16], A. B. Pearlman[17,18,29], J. X. Prochaska[19,20,21], S. D. Ryder[22,23], P. Scholz[24], R. M. Shannon[8], and N. Tejos[25]

[1] Center for Interdisciplinary Exploration and Research in Astrophysics (CIERA) and Department of Physics and Astronomy, Northwestern University, Evanston, IL 60208, USA; teftekhari@northwestern.edu
[2] Department of Astronomy, Columbia University, New York, NY 10027, USA
[3] Theoretical High Energy Astrophysics (THEA) Group, Columbia University, New York, NY 10027, USA
[4] ASTRON, Netherlands Institute for Radio Astronomy, Oude Hoogeveensedijk 4, 7991 PD Dwingeloo, The Netherlands
[5] Joint institute for VLBI ERIC, Oude Hoogeveensedijk 4, 7991 PD Dwingeloo, The Netherlands
[6] Anton Pannekoek Institute for Astronomy, University of Amsterdam, Science Park 904, 1098 XH Amsterdam, The Netherlands
[7] CSIRO, Space and Astronomy, PO Box 76, Epping, NSW 1710, Australia
[8] Centre for Astrophysics and Supercomputing, Swinburne University of Technology, John St, Hawthorn, VIC 3122, Australia
[9] European Space Agency (ESA), European Space Astronomy Centre (ESAC), Camino Bajo del Castillo s/n, E-28692 Villanueva de la Cañada, Madrid, Spain
[10] Cosmic Dawn Center (DAWN), Denmark
[11] Niels Bohr Institute, University of Copenhagen, Jagtvej 128, DK-2200 Copenhagen N, Denmark
[12] Department of Astronomy & Astrophysics, The Pennsylvania State University, University Park, PA 16802, USA
[13] Institute for Computational & Data Sciences, The Pennsylvania State University, University Park, PA 16802, USA
[14] Institute for Gravitation and the Cosmos, The Pennsylvania State University, University Park, PA 16802, USA
[15] Astronomy Department and Theoretical Astrophysics Center, University of California, Berkeley, CA 94720, USA
[16] Center for Computational Astrophysics, Flatiron Institute, 162 5th Ave, New York, NY 10010, USA
[17] Department of Physics, McGill University, 3600 rue University, Montréal, QC H3A 2T8, Canada
[18] Trottier Space Institute, McGill University, 3550 rue University, Montréal, QC H3A 2A7, Canada
[19] Department of Astronomy and Astrophysics, University of California, Santa Cruz, CA 95064, USA
[20] Kavli Institute for the Physics and Mathematics of the Universe (Kavli IPMU), 5-1-5 Kashiwanoha, Kashiwa 277-8583, Japan
[21] Division of Science, National Astronomical Observatory of Japan, 2-21-1 Osawa, Mitaka, Tokyo 181-8588, Japan
[22] School of Mathematical and Physical Sciences, Macquarie University, NSW 2109, Australia
[23] Astrophysics and Space Technologies Research Centre, Macquarie University, Sydney, NSW 2109, Australia
[24] Dunlap Institute for Astronomy & Astrophysics, University of Toronto, 50 St. George St., Toronto, ON M5S 3H4, Canada
[25] Instituto de Física, Pontificia Universidad Católica de Valparaíso, Casilla 4059, Valparaíso, Chile
Received 2023 July 7; revised 2023 September 6; accepted 2023 September 8; published 2023 November 14

Abstract

We present the first X-ray census of fast radio burst (FRB) host galaxies to conduct the deepest search for active galactic nuclei (AGN) and X-ray counterparts to date. Our sample includes seven well-localized FRBs with unambiguous host associations and existing deep Chandra observations, including two events for which we present new observations. We find evidence for AGN in two FRB host galaxies based on the presence of X-ray emission coincident with their centers, including the detection of a luminous ($L_X \approx 5 \times 10^{42}$ erg s^{-1}) X-ray source at the nucleus of FRB 20190608B's host, for which we infer an SMBH mass of $M_{\rm BH} \sim 10^8\,M_\odot$ and an Eddington ratio $L_{\rm bol}/L_{\rm Edd} \approx 0.02$, characteristic of geometrically thin disks in Seyfert galaxies. We also report nebular emission-line fluxes for 24 highly secure FRB hosts (including 10 hosts for the first time), and assess their placement on a BPT diagram, finding that FRB hosts trace the underlying galaxy population. We further find that the hosts of repeating FRBs are not confined to the star-forming locus, contrary to previous findings. Finally, we place constraints on associated X-ray counterparts to FRBs in the context of ultraluminous X-ray sources (ULXs), and find that existing X-ray limits for FRBs rule out ULXs brighter than $L_X \gtrsim 10^{40}$ erg s^{-1}. Leveraging the CHIME/FRB catalog and existing ULX catalogs, we search for spatially coincident ULX–FRB pairs. We identify a total of 28 ULXs spatially coincident with the localization regions for 17 FRBs, but find that the DM-inferred redshifts for the FRBs are inconsistent with the ULX redshifts, disfavoring an association between these specific ULX–FRB pairs.

Unified Astronomy Thesaurus concepts: Radio transient sources (2008); Active galactic nuclei (16); Ultraluminous x-ray sources (2164); AGN host galaxies (2017)

1. Introduction

Fast radio bursts (FRBs) are bright, millisecond-duration flares of coherent radio emission (Lorimer et al. 2007; Thornton et al. 2013) whose large dispersion measures (DMs) point to an extragalactic origin. Despite over 500 FRBs published in the literature to date (e.g., Macquart et al. 2020; CHIME/FRB Collaboration et al. 2020, CHIME/FRB Collaboration et al. 2023; Law et al. 2023), the sources

[26] NASA Einstein Fellow.
[27] Veni Fellow.
[28] ESA Research Fellow.
[29] Banting Fellow, McGill Space Institute (MSI) Fellow, and FRQNT Postdoctoral Fellow.

responsible for producing FRBs are highly debated, in large part due to the dearth of well-localized events (Eftekhari & Berger 2017) as well as the fact that some FRBs have been known to repeat (so-called "repeaters;" Spitler et al. 2016) while others appear as one-off events (Shannon et al. 2018; CHIME/FRB Collaboration et al. 2021). Although repeating and apparently nonrepeating FRBs exhibit a number of distinctions in their spectrotemporal properties (Pleunis et al. 2021)—and potentially their host galaxy properties (Gordon et al. 2023)—analyses of the FRB population cannot exclude the possibility that all FRBs intrinsically repeat (James 2023).

To reconcile this apparent diversity in burst properties and environments, a wide range of theoretical models have been put forth for FRB progenitors, ranging from compact object mergers (Margalit et al. 2019; Sridhar et al. 2021), and flares from highly magnetized stars (Margalit & Metzger 2018), to the super-Eddington accretion onto a neutron star or black hole (Sridhar et al. 2021, 2022), or even more exotic phenomena invoking cosmic strings (Costa et al. 2018) and primordial black holes (Abramowicz et al. 2018). At present, prevailing theoretical models invoke magnetars, whose extremely large magnetic fields are capable of storing enormous magnetospheric energies released in FRB flashes. Indeed, the discovery of a luminous, millisecond-duration burst from the known Galactic magnetar SGR 1935+2154 (CHIME/FRB Collaboration et al. 2020; Bochenek et al. 2020) supports a connection between extragalactic magnetars and FRBs (Margalit et al. 2020). Recent studies suggest that magnetars which formed via multiple formation channels—and not strictly through core-collapse supernovae—likely contribute to the known FRB population (e.g., Margalit et al. 2019; Kirsten et al. 2022; Pelliciari et al. 2023).

Technical upgrades to a number of FRB experiments in recent years have facilitated a small, but growing number of (sub)arcsecond localizations and robust host galaxy identifications for approximately three dozen events (e.g., Bhardwaj et al. 2021; Kirsten et al. 2022; Gordon et al. 2023; Law et al. 2023; Ravi et al. 2023; Ryder et al. 2023; Sharma et al. 2023). The first population studies demonstrate that FRB hosts span a wide range of stellar masses and star formation rates (SFRs) and trace the underlying population of field galaxies (Heintz et al. 2020; Bhandari et al. 2022; Gordon et al. 2023).

These early host galaxy compilations have also revealed that a nonnegligible fraction of FRB hosts occupy a distinct region of the Baldwin–Phillips–Terlevich (BPT; Baldwin et al. 1981) diagram, pointing to emission-line ratios in excess of typical star-forming galaxies (Heintz et al. 2020; Bhandari et al. 2022; Ibik et al. 2023). In particular, nonrepeating FRBs seem to indicate a preference for a subpopulation of low-ionization nuclear emission-line region (LINER) galaxies, while repeating FRBs lie exclusively along the star-forming branch. This distinction suggests that nonrepeating FRBs may be preferentially located in environments with enhanced levels of photoionization.

The nature of LINER galaxies, however, and the source of their ionizing photons have been under debate since their discovery (Heckman 1980). Existing theories associate LINERs with low-luminosity active galactic nuclei (AGN) or stellar ionization from evolved post–asymptotic giant branch stars (Singh et al. 2013). For FRB hosts, the latter scenario would implicate older stellar populations and hence FRB progenitors formed through channels with large average delay times between star formation and FRB source formation (e.g., short-duration gamma-ray bursts). Conversely, if the hard radiation fields observed in some FRB hosts are driven by central AGN, pointing to an elevated fraction of AGN in FRB hosts, this would lend support for theories that presuppose an enhanced rate of compact objects formed in AGN accretion disks (Cantiello et al. 2021; Perna et al. 2021a, 2021b; Jermyn et al. 2021) or FRB progenitor models that invoke AGN (Zhang 2017). Indeed, several of these theories have been put forth for relativistic transients, including both long- and short-duration gamma-ray bursts, but could be applied here given the higher stellar densities in AGN disks in general. Moreover, with only a small sample of FRB hosts that have been analyzed in this context (Heintz et al. 2020; Bhandari et al. 2022), a larger study is warranted to quantify the true occurrence rate of AGN (and LINER galaxies) in FRB hosts.

Concurrent to discerning the origin of the hard radiation fields prevalent in FRB hosts, X-ray observations can uniquely probe high-energy counterparts to FRBs. Constraints on periodicity in the burst rate from two repeating FRBs (Rajwade et al. 2020; CHIME/FRB Collaboration et al. 2020) have prompted theories that they are powered by relativistic flares along precessing jets associated with accretion onto compact objects (Sridhar et al. 2021). The observed (millisecond) durations and the extreme luminosities of typical FRBs, as well as the properties of their host galaxies, suggest that FRBs may be produced by stellar-mass ultraluminous X-ray sources (ULXs) powered by super-Eddington accretion onto a compact object (Sridhar et al. 2021). Within this framework, bright ULX-like X-ray emission should be associated with at least some FRBs. While deep limits on X-ray counterparts exist for a small number of well-localized FRB sources (e.g., Scholz et al. 2020; Kirsten et al. 2022; Pearlman et al. 2023) and targeted searches for FRBs from nearby galaxies hosting ULXs have been conducted (Pelliciari et al. 2023), there have been no concerted efforts thus far to search for ULXs coincident with the localization regions of the hundreds of FRBs detected across the sky.

Here we report the X-ray properties for all well-localized FRBs with existing Chandra X-ray observations (including newly obtained data for two events) to probe the presence of both AGN in FRB hosts and X-ray counterparts at the FRB locations. Our sample consists of seven FRBs, including five repeating sources. In Section 2, we present our observations and data reduction, which includes new Karl G. Jansky Very Large Array (VLA) observations for two FRBs. In Section 3, we combine radio and X-ray observations of our sample of hosts to constrain the multiwavelength properties of AGN in FRB host galaxies. We additionally present an updated BPT analysis for a uniformly modeled sample of 22 FRB host galaxies (in addition to two hosts from the literature). We leverage the X-ray observations to place limits on associated X-ray counterparts to FRBs in Section 4, and we further explore a possible connection between FRBs and ULXs by searching for FRBs beyond the original sample that are spatially coincident with cataloged ULXs. We summarize our results in Section 5. Throughout the paper, we use the latest Planck cosmological parameters for a flat Λ cold dark matter (ΛCDM) Universe, with $H_0 = 67.66$ km s^{-1} Mpc^{-1}, $\Omega_m = 0.310$, and $\Omega_\lambda = 0.690$ (Planck Collaboration et al. 2020).

Table 1
X-Ray and Radio Observations of the Host Galaxies of Localized FRBs

FRB	z	Average Observation Epoch (MJD)	Exposure Time (ks)	$\log(L_{2-10\ \mathrm{keV}})$ (erg s^{-1})	$\log(L_{5\ \mathrm{GHz}})$ (erg s^{-1})	N_H (10^{22} cm^{-2})	References
FRB 20121102A	0.1927	2016 Nov 30	99.9[a]	<41.2	39.1	0.63	1, 2, 3, 4
FRB 20180916B	0.0337	2019 Dec 10	32.7[b]	<40.0	<36.1	0.61	5, 6
FRB 20190520B	0.2418	2020 Sept 14	14.9	<41.9	39.1	0.26	7, 8
FRB 20190608B	0.1178	2021 Dec 06	19.8	$42.7^{+0.06}_{-0.06}$	38.1	0.06	This work, 9
FRB 20200120E	0.0008	2010 Jan 24	1205.3[c]	$40.4^{+0.003}_{-0.003}$	37.0	0.04	10, 11, 12
FRB 20200430A	0.1608	2022 Apr 24	34.8[d]	<41.4	<37.7	0.04	This work
FRB 20201124A	0.0982	2021 Apr 20	29.7	$40.6^{+0.16}_{-0.16}$	38.2	0.45	13

Notes. X-ray luminosity limits and detections correspond to the host center. Limits at the FRB position for each source are given in Section 2. Limits correspond to 3σ.
[a] The total exposure time was spread across four epochs spanning 2015 Nov 23–2017 Nov 01.
[b] The total exposure time was spread across two epochs spanning 2019 Dec 03–2019 Dec 18.
[c] The total exposure time was spread across 58 epochs spanning 2000 May 07–2022 Jun 04.
[d] The total exposure time was spread across two epochs spanning 2022 Apr 23–2022 Apr 24.
References: (1) Scholz et al. (2016); (2) Chatterjee et al. (2017); (3) Scholz et al. (2017); (4) PI: S. Bogdanov; (5) Scholz et al. (2020); (6) Marcote et al. (2020); (7) J. Sydnor et al. (2023, in preparation); (8) Niu et al. (2022); (9) Bhandari et al. (2020); (10) Kirsten et al. (2022); (11) see *Facilities* statement; (12) Miller et al. (2010); and (13) Piro et al. (2021).

2. Observations

2.1. Sample Selection

Our sample of FRB hosts includes all well-localized (∼a few to hundreds of milliarcseconds) events with unambiguous host associations (a probabilistic association of transients to their hosts (PATH); Aggarwal et al. 2021; with posterior probability $\gtrsim 90\%$) and existing Chandra data. The resulting sample spans a redshift range of $z \sim 0.0$–0.2418[30] and includes five FRBs with previously published X-ray data which we reanalyze here and two for which we present new Chandra observations (see Table 1). The FRB hosts in our sample span a wide range in both stellar masses ($\sim\log(M_*/M_\odot) = 8.14 - 10.84$) and SFRs ($\sim 0.04$–$7.03\,M_\odot\,\mathrm{yr}^{-1}$), similar to the general population of FRB hosts (Gordon et al. 2023), although are biased toward repeating events (five out of seven FRBs).

2.2. X-Ray Detection of the AGN in the Host Galaxy of FRB 20190608B

We obtained X-ray observations with the Chandra Advanced CCD Imaging Spectrometer (ACIS-S; Obs ID: 25251; PI: T. Eftekhari) of the field of FRB 20190608B (a nonrepeating FRB discovered and localized by the Australian Square Kilometre Array Pathfinder (ASKAP; Macquart et al. 2020) on UT 2021 December 6 with an exposure time of 19.8 ks. We analyzed the data using the `CIAO` software package (v4.13) and followed standard ACIS data filtering.

We detect a bright X-ray source offset from the FRB position by $\approx 1\farcs6$ with high significance (71σ) using a blind search with `wavdetect` (Figure 1). The source is detected in an elliptical region of size $2\farcs8 \times 2\farcs5$ (PA = 32°) centered at R.A. = $22^{\rm h}16^{\rm m}04\fs858$, decl. = $-7^{\rm d}53^{\rm m}56\fs297$. To estimate the background, we create a 35″ radius region near the center of the chip and free from any obvious sources. We find a net source count rate of $(108.3 \pm 7.5) \times 10^{-4}$ counts s^{-1} (0.5–8 keV). Given the spatial coincidence of the source with the host galaxy center and the unextended nature of the X-ray emission, we consider the source a putative AGN.

We rebin the spectrum across the $2\farcs8 \times 2\farcs5$ source region using 2 counts bin^{-1} and fit the data using an absorbed power-law model (`tbabs*ztbabs*pow` in `Xspec`; Arnaud 1996) with a fixed Galactic absorption column density $N_{\rm H,MW} = 5.9 \times 10^{20}\,\mathrm{cm}^{-2}$ (Willingale et al. 2013), solar abundances from Asplund et al. (2009), and use the maximum likelihood C-statistic for Poisson statistics (`c-stat`; Cash 1979). We find a photon index of $\Gamma = 1.9 \pm 0.3$ (68% confidence) and an intrinsic column density $N_{\rm H} = (4.7 \pm 0.4) \times 10^{21}\,\mathrm{cm}^{-2}$ for the AGN in the host galaxy. The model fit is shown in the right panel of Figure 1. To measure the quality of the fit, we use the Cramer–von Mises (CvM) test statistic (`statistic test cvm`; Cramér 1928; Mises 1928) and `XSPEC`'s "goodness" simulations to simulate realizations of the power law and determine what percentage of simulations has test statistics smaller than that of the data. A value of ∼50% indicates that the observed spectrum was produced by the model. We find that 43% of the realizations have a lower CvM statistic than the data, indicating the model is a good fit. Applying these spectral parameters to the net count rate and employing `cflux`, we find an unabsorbed X-ray flux $F_X = (1.4 \pm 0.2) \times 10^{-13}\,\mathrm{erg\,cm^{-2}\,s^{-1}}$ (2–10 keV), corresponding to an X-ray luminosity $L_{\rm X} = (5.4 \pm 0.8) \times 10^{42}\,\mathrm{erg\ s^{-1}}$ at the redshift of the FRB host, $z = 0.1178$ (see Table 1).

To determine the location of the X-ray source relative to the host galaxy center, any substructure within the host galaxy, and the position of FRB 20190608B, we use the Hubble Space Telescope (HST) F300X image of the host galaxy (Chittidi et al. 2021), which enables a precise host centroid. Since there are not enough sources in common between the HST and Chandra images, we use a Dark Energy Camera Legacy Survey image (DECaLS; DR10; Dey et al. 2019) to obtain a common absolute astrometric frame. First, we perform relative astrometry between the HST image using `Source Extractor` (Bertin & Arnouts 1996) and point sources in common. We then register the Chandra field of view to the DECaLS astrometric system using sources in common. With both the HST and Chandra images tied to the same astrometric frame, we find that the X-ray source is coincident with the host galaxy center (Figure 1).

The observed properties of the X-ray source, namely its spatial coincidence with the host galaxy center, luminous X-ray

[30] The $z = 0$ source corresponds to FRB 20200120E located in the nearby M81 galaxy at $d = 3.6$ Mpc (Kirsten et al. 2022).

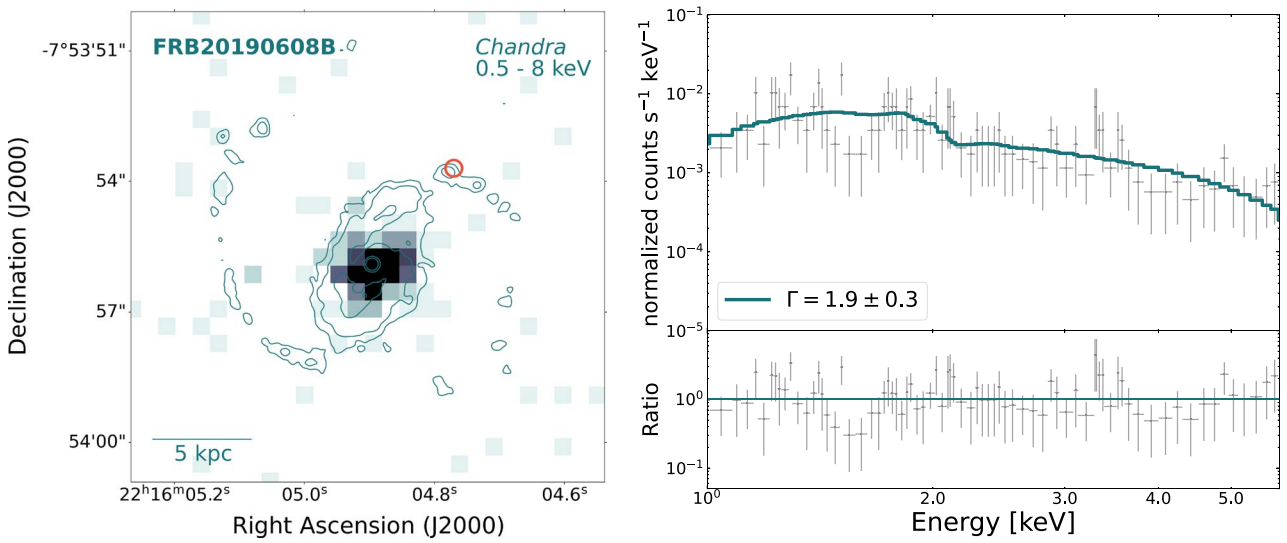

Figure 1. Left: Chandra X-ray detection (0.5–8 keV) of the host galaxy of FRB 20190608B. Contours from the Gaussian-smoothed HST (F300X) data (Chittidi et al. 2021) are overlaid in green. The red circle corresponds to the 1σ positional uncertainty on the FRB position (Day et al. 2021). Right: X-ray spectrum (gray points) of the AGN in the host galaxy of FRB 20190608B, modeled with an absorbed power law (green curve) with a best-fit power-law index $\Gamma = 1.9 \pm 0.3$.

emission at the level of $L_X = 5.4 \times 10^{42}$ erg s^{-1}, and an X-ray spectrum that is well characterized by an absorbed power law, indicate that the X-ray source is powered by an AGN. We note that we do not detect any counts at the FRB position, corresponding to a 3σ upper limit on the absorbed X-ray flux of $F_X < 3 \times 10^{-15}$ erg cm^{-2} s^{-1} (2–10 keV).

2.3. Constraints on an AGN in the Host Galaxy of FRB20200430A

We obtained Chandra observations (PI: T. Eftekhari) of FRB 20200430A (a nonrepeating FRB detected and localized by ASKAP; Heintz et al. 2020) in two separate epochs with exposure times of 22.9 and 11.9 ks on UT 2022 April 23 (Obs ID: 25252) and 24 (Obs ID: 26397), respectively. We do not blindly detect X-ray emission at or near the position of FRB 20200430A in either epoch using `wavdetect`. We therefore generate a coadded, exposure-corrected image using `merge_obs` and perform a targeted extraction around the host center using an aperture radius of 1″. We perform background estimation in a similar manner to FRB 20190608B. The source is not detected in the merged event file corresponding to a 3σ upper limit on the count rate of 3.6×10^{-4} counts s^{-1} (assuming Poisson statistics; Gehrels 1986). For $\Gamma = 2$ (typical of AGN in nearby galaxies; Ho 2008) and $N_{\rm H,MW} = 3.5 \times 10^{20}$ cm^{-2}, the 3σ limit on the 2−10 keV absorbed X-ray flux is $F_X < 3.2 \times 10^{-15}$ erg cm^{-2} s^{-1}, corresponding to an X-ray luminosity $L_X < 2.8 \times 10^{41}$ erg s^{-1}. We derive the same flux limit at the FRB position located ∼1″ from the host center.

2.4. Reanalysis of Archival Data

We also searched the positions of all localized FRBs in the Chandra archive to compile a complete list of X-ray observations for well-localized events (see Table 1). We find five FRBs with robust host galaxy associations with archival Chandra data (FRBs 20121102A, 20180916B, 20190520B, 20200120E, and 20201124A). With the exception of FRB20200120E, all of these were targeted for FRB science. For uniformity, we reanalyze the data using the above methodology. In all cases, hydrogen column densities are derived using the method of Willingale et al. (2013) and X-ray fluxes are estimated assuming a photoelectrically absorbed power-law spectrum with $\Gamma = 2$.

For FRB 20121102A, we combine four epochs of existing Chandra observations, including one ACIS-S exposure from 2015 November (Obs ID:18717; PI: P. Scholz) and three ACIS-I exposures from 2016 November and 2017 January and November (Obs ID: 19286, 19287, and 19288; PI: S. Bogdanov) corresponding to a total exposure time of 99.99 ks. Only two photons are detected within a 1″ radius aperture centered on the host position, consistent with a nondetection. The 3σ upper limit on the count rate from Poisson statistics is $<1.09 \times 10^{-4}$ counts s^{-1}. For $N_{\rm H,MW} = 6.3 \times 10^{21}$ cm^{-2}, the 3σ limit on the absorbed flux is $F_X < 1.2 \times 10^{-15}$ erg cm^{-2} s^{-1} (2–10 keV), corresponding to an X-ray luminosity $L_X < 1.6 \times 10^{41}$ erg s^{-1}. We derive the same flux limit at the FRB position.

We independently analyze the two existing epochs of Chandra observations for FRB 20180916B following Scholz et al. (2020). We find four counts in a 1″ radius aperture centered on the FRB host position. Accounting for the background, the total source counts are 2.02 ± 1.01 (0.8σ significance), consistent with a nondetection. The 3σ Poisson upper limit on the count rate is 3.3×10^{-4} counts s^{-1}. For $N_{\rm H,MW} = 6.1 \times 10^{21}$ cm^{-2}, the 3σ limit on the absorbed flux is $F_X < 3.4 \times 10^{-15}$ erg cm^{-2} s^{-1} (2–10 keV), corresponding to an X-ray luminosity $L_X < 9.9 \times 10^{41}$ erg s^{-1}. At the FRB position (offset from the host galaxy center by ≈7.″8), we find a single count in a 1″ radius aperture, consistent with a nondetection. The 3σ Poisson upper limit on the count rate is therefore 2.7×10^{-4} counts s^{-1}, corresponding to a 3σ limit on the absorbed flux of $F_X < 2.8 \times 10^{-15}$ erg cm^{-2} s^{-1} (2–10 keV).

For FRB 20190520B, we analyze a single ACIS-S 14.9 ks exposure (Obs ID: 22370; PI: K. Aggarwal; Sydnor et al. 2023). We do not detect any counts in a 1″ radius aperture centered on the host center. The 3σ upper limit on the count rate is 4.4×10^{-4} counts s^{-1}. For $N_{\rm H,MW} = 2.56 \times 10^{21}$ cm^{-2}, the 3σ limit on the X-ray flux is $F_X < 3.7 \times 10^{-15}$ erg cm^{-2} s^{-1} (2–10 keV), corresponding to an X-ray luminosity

$L_X < 8.6 \times 10^{41}$ erg s^{-1}. We derive the same flux limit at the FRB position.

For FRB 20201124A, we detect five counts in a 1.″5 radius aperture centered on the host position in a 29.7 ks exposure (Obs ID:25016; PI: L. Piro; Piro et al. 2021). We find a net source count rate of $(1.6 \pm 0.7) \times 10^{-4}$ counts s^{-1} (2.4σ significance), consistent with a marginal detection, as reported in Piro et al. (2021). We convert this count rate to an X-ray flux with $N_{\rm H,MW} = 4.5 \times 10^{21}$ cm^{-2} and find $F_X = (1.6 \pm 0.6) \times 10^{-15}$ erg cm^{-2} s^{-1} (2–10 keV). At the distance of FRB 20201124A ($z = 0.0982$), the corresponding X-ray luminosity is $L_X = (4 \pm 1.7) \times 10^{40}$ erg s^{-1}, consistent with the values reported in Piro et al. (2021) and a star formation origin, as demonstrated in their work. Given the small spatial offset between the FRB and the host center (0.″7), we adopt the host galaxy X-ray flux as an upper limit for X-ray emission at the FRB position.

In the case of FRB 20200120E (located in M81, which has been observed extensively at X-ray wavelengths), we separately compile and merge all existing Chandra ACIS observations that cover the host and FRB position[31] using the python code `superchandra.py` (Kilpatrick 2023), which allows us to easily query and analyze all Chandra observations at a given set of input coordinates. We note that none of the ACIS observations comprising our merged event files were targeted for FRB science. We derive an absorbed X-ray flux at the host center (15″ aperture radius) of $F_X = (1.52 \pm 0.01) \times 10^{-11}$ erg cm^{-2} s^{-1} (2–10 keV) for $N_{\rm H,MW} = 4 \times 10^{20}$ cm^{-2}, corresponding to an X-ray luminosity $L_X = (2.36 \pm 0.02) \times 10^{40}$ erg s^{-1}. Here, $N_{\rm H,MW}$ is derived with the `superchandra.py` script using the known linear relation between the line-of-sight optical extinction A_V (Schlafly & Finkbeiner 2011) and the hydrogen column density (Güver & Özel 2009). We do not detect any counts in a 1″ radius aperture at the FRB position, corresponding to a 3σ limit on the absorbed X-ray flux of $F_X < 8.6 \times 10^{-15}$ erg cm^{-2} s^{-1} (2–10 keV; see also Pearlman et al. 2023).

2.5. Radio Continuum Observations

We obtained radio observations of FRBs 20200430A (20A-157; PI: S. Bhandari) and 20190608B (22B-115; PI: T. Eftekhari) with the VLA at 6 GHz (*C* band) and 22 GHz (*K* band) on UT 2020 September 4 and UT 2022 April 24, respectively. The field of FRB 20200430A was observed in the B-configuration with a total on-source integration time of ∼1 hr. FRB 20190608B was observed in the A-configuration with a total on-source integration time of 56 minutes. Both observations utilized the 3-bit samplers providing the full 4 GHz of bandwidth at *C* band and 8 GHz of bandwidth at *K* band, not accounting for the excision of edge channels and RFI. For FRB 20200430A, we used 3C286 for the bandpass and flux density calibration and J1504+1029 for the complex gain calibration. For FRB 20190608B, we used 3C147 for the bandpass and flux density calibration and J2229-0832 for the complex gain calibration.

In both cases, we imaged the pipeline-calibrated measurement sets using 2048 × 2048 pixels at a scale of 0.″2 pixel^{-1} and 0.″02 pixel^{-1} at 6 and 22 GHz, respectively, using multifrequency synthesis (MFS; Sault & Wieringa 1994) and *w*-projection with 128 planes (Cornwell et al. 2008). We do not detect radio emission at the host center or the FRB location for either FRB, corresponding to rms values of 4.32 μJy (6 GHz) and 6.14 μJy (22 GHz) for FRB 20200430A and FRB 20190608B, respectively.

We note that FRB 20190608B was observed previously with the Australia Telescope Compact Array (ATCA) under project code C3211 (PI: R. M. Shannon) and with the VLA (19A-121; PI: S. Bhandari) at ∼6 GHz (Bhandari et al. 2020). A radio source is marginally detected in the ATCA observations with a flux density of $\sim 65 \pm 15$ μJy at 5.5 GHz. The VLA observations, taken in A-configuration, revealed resolved radio continuum emission with a peak brightness of ∼27 μJy beam^{-1} near the center of the host. The inferred SFR from the 5.5 GHz ATCA detection of $3.9^{+1.0}_{-0.9}$ $M_\odot$ yr^{-1} (using the relation of Greiner et al. 2016) is below the optically inferred SFR of $7.03^{+1.43}_{-1.15}$ $M_\odot$ yr^{-1} (Gordon et al. 2023), but we note that standard relations between radio flux and star formation result in differences of order a factor of two (e.g., Yun & Carilli 2002; Murphy et al. 2011). Moreover, given that the emission spans a range of spatial scales (as shown by comparing the peak brightness seen in the ATCA and VLA images), we emphasize that the radio flux densities should be regarded with caution. Indeed, for $\rm SFR_{radio} = 3.9\,M_\odot\,yr^{-1}$, the expected flux density at 22 GHz assuming a spectral index $\alpha = 0.7$ is ∼24 μJy, which is above our 3σ limit of 18 μJy. This "missing flux" at higher frequencies is consistent with the higher angular resolution in our VLA 22 GHz observations (∼0.″1) relative to the ATCA 5.5 GHz observations (20″ × 2″). Thus, we conclude that the most likely origin for the extended radio emission is star formation within the host galaxy.

We further supplement our sample of seven FRB hosts with radio continuum observations from the literature. This includes radio detections of the persistent radio sources (PRSs) associated with FRB 20121102A ($F_{6\ \rm GHz} = 203$ μJy; Chatterjee et al. 2017) and FRB 20190520B ($F_{3\ \rm GHz} = 202$ μJy; Niu et al. 2022); radio detections of the host galaxy of FRB 20201124A ($F_{6\ \rm GHz} = 221$ μJy; Ravi et al. 2022); and a radio limit for FRB 20180916B ($F_{1.6\ \rm GHz} < 18$ μJy (3σ); Marcote et al. 2020). For FRB 20200120E (M81), we adopt the average flux density ($F_{8.4\ \rm GHz} = 103.2$ mJy) over seven epochs of observations as reported in Miller et al. (2010). We list the radio luminosity for each source (*k*-corrected to rest-frame 5 GHz assuming $\alpha = 0.7$) in Table 1.

3. Multiwavelength Properties of the AGN in FRB Host Galaxies

3.1. The AGN in the Host of FRB20190608B

The host galaxy of FRB 20190608B (SDSS J221604.90-075355.9) is a grand design SB(r)c galaxy and is among the most massive ($\approx 3.6 \times 10^{10}\,M_\odot$) FRB hosts discovered to date (Gordon et al. 2023). While the FRB location is coincident with a knot of UV emission that is likely due to star formation (Chittidi et al. 2021), model fits to the full spectral energy distribution (SED) indicate it is one of two FRB hosts with a poststarburst star formation history in which the galaxy has undergone a recent quenching event (Gordon et al. 2023). Such galaxies commonly host supermassive black holes (SMBHs) which are believed to regulate star formation via AGN-driven feedback (Martín-Navarro et al. 2018). Here, we report the first detection of luminous X-ray emission spatially coincident with

[31] Details of the observations included in each merged event file are given in the *Facilities* statement at the end of the paper.

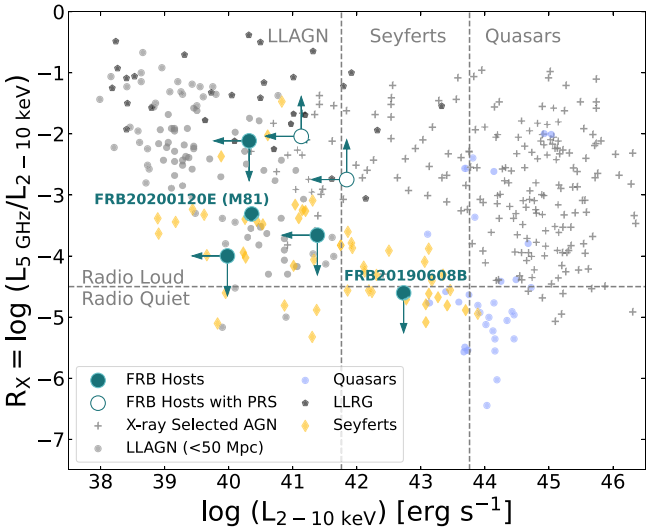

Figure 2. Rest-frame radio-to-X-ray luminosity ratio (R_X) as a function of rest-frame X-ray luminosity (L_X) for FRB hosts (teal circles). Open circles correspond to FRBs with coincident PRSs, where we conservatively adopt the PRS luminosity as an upper limit on the radio luminosity of an associated AGN. Shown for comparison are values for field AGN, including LLAGN (She et al. 2017; Gross et al. 2019), X-ray selected AGN (Ballo et al. 2012; LaMassa et al. 2016), quasars (Kellermann et al. 1989; Piconcelli et al. 2005; Gross et al. 2019), Seyferts (Ho & Peng 2001; Terashima & Wilson 2003; Panessa et al. 2007), and LLRGs (Chiaberge et al. 2005; Balmaverde & Capetti 2006). Vertical dashed lines denote the nominal divisions between LLAGN and Seyferts at $\log(L_X \sim 41.76$ erg s$^{-1})$ and Seyferts and quasars at $\log(L_X \sim 43.76$ erg s$^{-1})$. The horizontal dashed line at $R_X = 4.5$ roughly divides radio-loud and radio-quiet AGN.

the center of the host of FRB 20190608B. An AGN origin is consistent with the previous detection of broad Hα emission in the optical spectrum, indicative of a Type I Seyfert galaxy (Stern & Laor 2012; Chittidi et al. 2021). As such, the host of FRB 20190608B is the only one known to harbor a Type I AGN. Our X-ray detection provides further evidence for an AGN origin (Figure 1).

In Figure 2, we plot the rest-frame radio-to-X-ray luminosity ratio $R_X = \log(L_{5\mathrm{GHz}}/L_{2-10\mathrm{keV}})$ as a function of rest-frame X-ray luminosity $L_X = L_{2-10\,\mathrm{keV}}$ for FRB 20190608B, where we conservatively adopt the 5.5 GHz flux density of the host previously ascribed wholly to star formation as an upper limit on any radio emission due to an AGN (see Section 2). For comparison, we also plot the values for several AGN samples from the literature, including low-luminosity AGN (LLAGN; $d < 50$ Mpc; She et al. 2017; Gross et al. 2019), X-ray-selected AGN (Ballo et al. 2012; LaMassa et al. 2016), quasars (Kellermann et al. 1989; Piconcelli et al. 2005; Gross et al. 2019), Seyferts (Ho & Peng 2001; Terashima & Wilson 2003; Panessa et al. 2007), and low-luminosity radio galaxies (LLRGs;[32] Chiaberge et al. 2005; Balmaverde & Capetti 2006). Vertical dashed lines at $log(L_X) = 41.76$ and $log(L_X) = 43.76$ erg s^{-1} roughly divide AGN into three luminosity regimes corresponding to LLAGN, Seyferts, and quasars (Brusa et al. 2007). We note however that Seyfert galaxies, particularly Type 2 Seyferts, can extend to much lower X-ray luminosities (Panessa et al. 2007), as shown in Figure 2.

[32] LLRGs are canonically unresolved, nonthermal radio cores in galaxies with optical classifications spanning Type 1 Seyferts, Type 2 Seyferts, and LINER galaxies.

Our X-ray detection of the host of FRB 20190608B, coupled with a limit on the radio emission, places this source in the region corresponding to Seyfert galaxies, consistent with its optical classification. The value of $R_X < -4.6$ is just below the nominal division between radio-loud and radio-quiet AGN ($R_X = -4.5$; Terashima & Wilson 2003), although a diverse range of morphologies and properties for radio AGN challenge a simple classification (Panessa et al. 2019). The increase in R_X for LLAGN with $L_X \lesssim 10^{42}$ erg s^{-1} may indicate the presence of an advection-dominated accretion flow in these objects (Terashima & Wilson 2003), as was inferred for the LLAGN in M81 (Xu & Cao 2009) and consistent with its placement in this diagram.

We use the velocity dispersion at the center of the galaxy as derived from a Gaussian fit to the Hβ line ($\sigma = 108$ km s^{-1}; Chittidi et al. 2021) and the M–σ relation of Zubovas & King (2012) for spiral galaxies to estimate the mass of the central SMBH. We infer an SMBH mass of $M_{\mathrm{BH}} \sim 10^8\,M_\odot$. For a derived stellar mass of $3.6 \times 10^{10}\,M_\odot$, the inferred black hole mass is consistent with scaling relations between central black hole masses and galaxy stellar masses (Kormendy & Ho 2013; Reines & Volonteri 2015). Finally, adopting a bolometric correction of $L_{\mathrm{bol}} = 16\,L_X$ (Ho 2008), we find an Eddington ratio of $L_{\mathrm{bol}}/L_{\mathrm{Edd}} \approx 0.02$, typical of Seyfert galaxies (Ho 2008). Moreover, this is consistent with the inferred value of $R_X < -4.6$ (and placement within the radio-quiet regime) for the host of FRB 20190608B and reflects the fact that geometrically thin disks, which are prevalent in Seyfert galaxies, are less efficient at jet production when compared to LLAGN (Terashima & Wilson 2003).

3.2. X-Ray Constraints on AGN in the FRB Host Population

Based on the Chandra X-ray observations presented here and compiled from the literature, we find evidence for AGN in two FRB host galaxies: the host of FRB 20190608B (Section 3.1) and the host of FRB 20200120E (M81), which was already known to harbor an LLAGN (Miller et al. 2010). We note that X-ray emission is also detected from the host of FRB 20201124A but is consistent with a star formation origin (Piro et al. 2021). The detection of AGN in two out of seven FRB hosts corresponds to an occurrence rate of ∼29%. Alternatively, if we consider the hosts of repeating and nonrepeating events separately, we find occupation fractions of ∼20% and ∼50%, respectively. Conversely, the AGN fraction in the local Universe is low, ranging from 0.1% at $z \sim 0.2$ to 1% at $z \sim 0.7$ (Martini et al. 2009). At face value, it seems that host galaxies which harbor AGN are overrepresented compared to galaxies at similar redshifts. However, existing deep X-ray observations of FRB host galaxies are extremely sparse, with uncharacterized selection effects. Thus a robust assessment of the true AGN occupation fraction in FRB hosts is not yet tenable. Given that the two AGN in FRB hosts are found in both repeating and nonrepeating FRB host galaxies, we observe no trend in the prevalence of AGN with FRB type, albeit based on a small sample size.

To place constraints on the presence of AGN in the absence of X-ray detections, we combine the Chandra limits with radio observations (see Table 1) to plot the radio-to-X-ray luminosity R_X against the X-ray luminosity L_X for the remainder of sources in Figure 2. We find that the X-ray limits for the majority of FRBs in our sample allow us to rule out any AGN with $L_X \lesssim 10^{41}$–10^{42} erg s^{-1}, including some LLAGN. However, we

cannot rule out the low-luminosity end of the LLAGN population centered around $L_X \sim 10^{39}$ erg s^{-1}, well below the sensitivity of existing X-ray observations for FRBs. For FRB 20200430A, our X-ray limit of $L_X < 2.5 \times 10^{41}$ erg s^{-1} allows us to rule out luminous quasars and most X-ray selected AGN, but we note that we cannot exclude the possibility of a Seyfert host.

Existing radio limits for FRB hosts, coupled with X-ray nondetections, correspond to radio-to-X-ray luminosity ratios of $R_X > -4$, and hence do not reach the regime of radio-quiet AGN. For FRBs 20121102A and 20190520B, the detection of coincident PRSs allows us to leverage the PRS luminosities as conservative upper limits on the radio luminosity of an associated AGN. While we cannot exclude the possibility of radio-loud LLAGN in these FRB hosts, we note that such sources are intrinsically rare in dwarf galaxies (e.g., Reines et al. 2020). We further note that for FRB 20200120E (M81), and indeed all FRBs in our sample (with the exception of FRB 20190608B), the radio and X-ray luminosities and limits are consistent with LLAGN.

3.3. Optical Emission-line Diagnostics for FRB Hosts

To determine the dominant source of ionization and distinguish between star-forming, LINER, and AGN galaxies in FRB hosts, we extract the nebular line fluxes for 22 highly secure FRB host galaxies (including 10 hosts for the first time; see Table 2) with high-quality spectra using the `Prospector` SED modeling code (Johnson et al. 2021) and following the prescription and sample selection of Gordon et al. (2023). We also include literature values for M81, the host of FRB 20200120E (Ho et al. 1996), and FRB 20220912A (Ravi et al. 2023).[33] We note that while SED fits exist for the host of FRB 20190711A, it is not included in our sample due to poor spectral data quality which precludes robust line emission diagnostics (Gordon et al. 2023). In Figure 3, we plot the emission-line ratios [O III] λ5007/Hβ λ4861 and [N II] λ6583/Hα λ6563 for FRB hosts on a BPT diagram (Baldwin et al. 1981) against the distribution of nearby ($0.02 < z < 0.4$) emission-line galaxies from the Sloan Digital Sky Survey (SDSS).

Using the standard demarcation lines between star-forming, AGN, and LINER galaxies for $z \lesssim 0.3$ (Kauffmann et al. 2003; Cid Fernandes et al. 2010), we find that the majority of FRB hosts occupy the star-forming region, consistent with their SED classifications (Gordon et al. 2023), and are largely aligned with the locus of star-forming galaxies. Moreover, our analysis of a larger sample of hosts demonstrates that the repeating FRB hosts do not lie exclusively in the star-forming region, in contrast to previous studies (Heintz et al. 2020; Bhandari et al. 2020), and that the hosts of both repeating and nonrepeating FRBs populate all three regions of the diagram roughly according to the underlying galaxy population.

To quantify this, we compare the FRB host galaxy population, and the host populations for repeating and nonrepeating events, to the distributions of star-forming, AGN, and LINER galaxies using 2D Kolmogorov–Smirnov (K-S) tests to determine whether they emerge from the same underlying population. We first employ a kernel density estimation (KDE) to the SDSS sample to divide the parent

[33] Line fluxes for FRBs 20200120E and 20220912A were obtained using a different method than the one we use here.

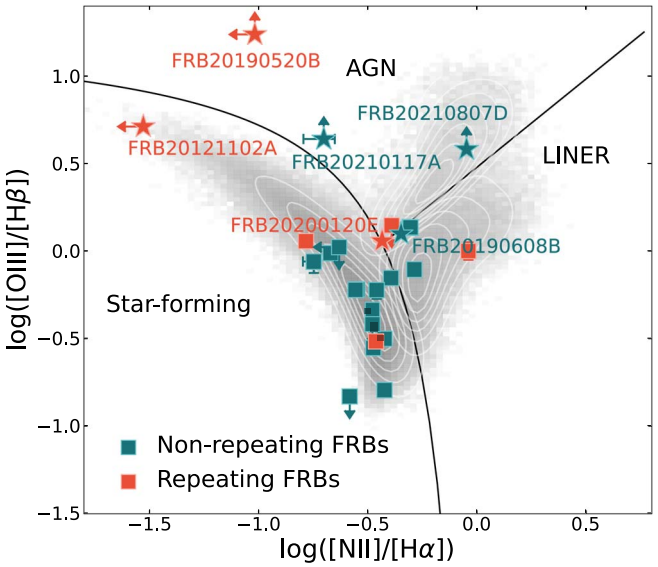

Figure 3. BPT classification diagram for FRB host galaxies, including repeating (orange) and nonrepeating (teal) events. Sources that are highlighted in the text are individually labeled and plotted as stars. Solid lines denote the typical demarcation between star-forming, AGN, and LINER galaxies (Kauffmann et al. 2003; Cid Fernandes et al. 2010). The gray-scale background corresponds to the density distribution of nearby ($0.02 < z < 0.4$) galaxies from SDSS. White contours show the KDE for each galaxy population used to model their probability density functions.

population into individual galaxy classes. We next perform 2D K-S tests, comparing the host populations for repeating and nonrepeating events to each galaxy population, where we include all limits in the analysis. The results are summarized in Table 3.

Comparing the hosts of repeating and nonrepeating FRBs collectively to all galaxy types, we find $P_{\rm KS} = 0.058$, suggesting that we cannot reject the null hypothesis that FRB hosts are drawn from the same underlying galaxy population. We furthermore find that all FRB hosts are consistent with an underlying population of star-forming+LINER galaxies ($P_{\rm KS} = 0.121$), but statistically inconsistent with a population of AGN+LINER galaxies, indicating that star-forming galaxies are the dominant population.

With only three sources in the AGN locus (one of which is a limit), we reject the null hypothesis that FRB hosts are drawn from the same population as AGN. These objects include the hosts of FRB 20210807D, FRB 20210117A, and FRB 20190520B, although the latter does not exhibit detectable Hβ or [N II] emission. Indeed, its location as an outlier on the BPT diagram, coupled with a dwarf host and the presence of a coincident PRS (Niu et al. 2022), bear a striking similarity to FRB 20121102A (Chatterjee et al. 2017). However, it is worth noting that the location of a galaxy on the BPT diagram is highly sensitive to the gas-phase metallicity (Kumari et al. 2021; Garg et al. 2022). In particular, low-metallicity galaxies exhibit a lower nitrogen abundance and a higher collisional excitation rate for [O III], which leads to a decrease in the [N II] flux, and an increase in the [O III] flux, respectively (Garg et al. 2022). A third dwarf host, the host of FRB 20210117A, lies in a similar region of the diagram but hosts an apparently nonrepeating FRB and lacks a persistent radio counterpart (Bhandari et al. 2023).

Table 2
Nebular Emission-line Fluxes for FRB Hosts

FRB	Hα	Hβ	[N II] 6584 Å	[O III] 5007 Å
FRB20121102A	$2.04^{+0.08}_{-0.09}$	$0.78^{+0.06}_{-0.06}$	<0.06	$4.03^{+0.30}_{-0.30}$
FRB20180301A	$3.49^{+0.11}_{-0.10}$	$0.99^{+0.04}_{-0.04}$	$0.58^{+0.02}_{-0.02}$	$1.13^{+0.04}_{-0.04}$
FRB20180916B	$96.75^{+2.67}_{-2.68}$	<52.93	$39.45^{+1.06}_{-1.04}$	<74.20
FRB20180924B	$3.67^{+0.08}_{-0.08}$	$0.90^{+0.03}_{-0.02}$	$1.89^{+0.04}_{-0.04}$	$0.71^{+0.02}_{-0.02}$
FRB20181112A	$1.76^{+0.07}_{-0.07}$	$0.50^{+0.03}_{-0.03}$	$0.87^{+0.06}_{-0.08}$	$0.69^{+0.03}_{-0.03}$
FRB20190102C	$3.78^{+0.29}_{-0.29}$	$0.40^{+0.11}_{-0.09}$	<0.88	<0.42
FRB20190520B	$0.62^{+0.04}_{-0.04}$	<0.02	<0.06	$0.40^{+0.04}_{-0.05}$
FRB20190608B	$74.48^{+1.59}_{-1.63}$	$21.78^{+0.60}_{-0.55}$	$33.42^{+0.68}_{-0.74}$	$27.29^{+0.64}_{-0.60}$
FRB20190611B	$1.48^{+0.10}_{-0.10}$	$0.31^{+0.02}_{-0.02}$	$0.26^{+0.02}_{-0.03}$	$0.27^{+0.02}_{-0.04}$
FRB20190714A	$9.61^{+0.24}_{-0.22}$	$2.01^{+0.08}_{-0.08}$	$3.22^{+0.07}_{-0.08}$	$0.57^{+0.03}_{-0.03}$
FRB20191001A	$45.40^{+0.94}_{-0.91}$	$9.80^{+0.43}_{-0.41}$	$17.10^{+0.35}_{-0.35}$	$3.10^{+0.09}_{-0.09}$
FRB20200120E[a]	11,380	1980	4180	2260
FRB20200430A	$3.36^{+0.13}_{-0.14}$	$0.89^{+0.04}_{-0.05}$	$1.16^{+0.04}_{-0.05}$	$0.53^{+0.03}_{-0.06}$
FRB20200906A	$14.56^{+0.38}_{-0.35}$	$3.14^{+0.10}_{-0.10}$	$3.10^{+0.08}_{-0.08}$	$3.06^{+0.09}_{-0.08}$
FRB20201124A	$107.93^{+2.19}_{-2.13}$	$21.72^{+0.60}_{-0.62}$	$37.17^{+0.75}_{-0.73}$	$6.63^{+0.18}_{-0.18}$
FRB20210117A	$0.39^{+0.02}_{-0.02}$	…	$0.08^{+0.01}_{-0.01}$	$0.42^{+0.02}_{-0.03}$
FRB20210320C	$16.11^{+0.45}_{-0.45}$	$3.43^{+0.16}_{-0.15}$	$4.55^{+0.15}_{-0.14}$	$2.08^{+0.08}_{-0.08}$
FRB20210410D	$2.81^{+0.10}_{-0.11}$	$0.32^{+0.05}_{-0.05}$	$0.73^{+0.03}_{-0.04}$	<0.05
FRB20210807D	$22.89^{+0.49}_{-0.55}$	<4.08	$20.44^{+0.41}_{-0.41}$	$15.58^{+0.43}_{-0.39}$
FRB20211127I	$501.43^{+11.34}_{-12.26}$	$177.31^{+6.18}_{-6.87}$	$188.78^{+4.38}_{-4.72}$	$28.55^{+0.98}_{-1.76}$
FRB20211203C	$11.32^{+0.29}_{-0.27}$	$3.73^{+0.14}_{-0.15}$	$3.14^{+0.09}_{-0.08}$	$2.25^{+0.07}_{-0.07}$
FRB20211212A	$99.33^{+4.38}_{-4.44}$	<24.71	$33.02^{+1.69}_{-1.93}$	<9.51
FRB20220105A	$2.36^{+0.09}_{-0.09}$	$0.59^{+0.03}_{-0.03}$	$0.95^{+0.03}_{-0.04}$	$0.42^{+0.02}_{-0.02}$

Note. Fluxes are in units of 10^{-16} erg s^{-1} cm^{-2} and corrected for Galactic extinction. Not listed are the values for FRB 20220912A, for which we use the line ratios presented in Ravi et al. (2022). Limits correspond to 3σ.
[a] From Ho et al. (1996).

Table 3
2D K-S Tests for FRB Host Populations

Galaxy Type	P_{KS} (Repeaters)	P_{KS} (Nonrepeaters)	P_{KS} (All)
All Types	0.011	**0.168**	**0.058**
SF	0.010	0.011	0.003
AGN	<0.001	<0.001	<0.001
LINER	0.002	<0.001	<0.001
SF+LINER	0.009	**0.207**	**0.121**
AGN+LINER	0.002	<0.001	<0.001

Note. P-values derived from 2D K-S tests comparing the FRB host populations separately (repeaters and nonrepeaters) and collectively (all) to different galaxy populations according to the BPT diagram. Values in bold correspond to $P_{KS} > 0.05$. SF: star forming.

Hosts for the X-ray-confirmed AGN, FRBs 20190608B and 20200120E (M81), lie within the LINER region. While the precise origin of LINER emission is not settled, studies in the last few decades have shown that AGN are present in roughly $\sim 50\%$ of LINERs (Ho et al. 2001; Satyapal et al. 2004; Dudik et al. 2005). Here the presence of luminous X-ray emission coincident with the host nuclei for both sources points to a central AGN (as opposed to stellar ionization) as the mechanism driving the elevated levels of ionization relative to star-forming galaxies. While several other FRB hosts are located in the AGN/LINER regions, complementary X-ray constraints are lacking for these sources, with the exception of FRB 20180916B for which X-ray observations place a fairly deep limit on the presence of an AGN (see Section 2).

Our results are similar to previous findings in that we do find evidence for a subset of hosts residing in the LINER region and offset from the main locus of star-forming galaxies (Heintz et al. 2020; Bhandari et al. 2022). However, the larger sample presented here demonstrates that the hosts of repeating FRBs are not confined to the star-forming region, in contrast to these earlier studies. Indeed, our results show that the host galaxies for both repeating and nonrepeating FRBs are statistically consistent with the full underlying galaxy population, with star-forming galaxies comprising the dominant population.

4. FRBs from Accreting Compact Objects

4.1. Searching for X-Ray Counterparts

The discovery of an apparent modulation in the activity level of two luminous repeating FRB sources (FRB 20180916B, activity modulation period of 16 days; CHIME/FRB Collaboration et al. 2020; FRB 20121102A, activity modulation period of 160 days; Rajwade et al. 2020) has motivated progenitor theories invoking accreting stellar-mass compact objects (Waxman 2017; Deng et al. 2021; Sridhar et al. 2021) —most of which require super-Eddington mass transfer (in analogy with ULXs) to explain the luminous FRB population. In this scenario, a misalignment of the black hole spin axis with respect to the angular momentum axis of the accretion disk leads to Lens–Thirring precession of the disk and thus the jet axis (Middleton et al. 2019), driving periodicity in the FRB activity cycle on timescales of weeks to years. A prediction of this model is that FRBs—during their active cycle—should be accompanied by quasi-persistent X-ray counterparts.

While the discovery of periodicity is limited to only two FRBs thus far, it is useful to use our X-ray census to constrain the ULX-like progenitor scenario. In Figure 4 (left panel), we compare X-ray limits for the FRBs in our sample to the luminosity distribution for ULXs using the multimission catalog of ULXs from Walton et al. (2022). This catalog consists of 1843 ULX sources associated with 951 host galaxies compiled from XMM-Newton, Swift, and Chandra X-ray source catalogs. While the sample selection is highly nonuniform and incomplete, it represents the largest ULX catalog compiled to date.

Current ULX surveys only identify them out to average distances of 75 Mpc (maximum distance of $d_{max} \approx 700$ Mpc), while our X-ray limits on a few cosmological FRBs at $z \approx 0.0337$–0.1608 are deep enough to probe the bright end of the ULX luminosity function ($\approx 10^{40}$ erg s^{-1}). The deepest limit comes from the closest repeating FRB 20200120E (at 3.6 Mpc), localized to a globular cluster in the nearby M81 galaxy. The X-ray luminosity at the location of the FRB is $L_X \lesssim 1.3 \times 10^{37}$ erg s^{-1} (Kirsten et al. 2022), corresponding to $\sim$0.01–0.1 L_{Edd} for a 10 $M_\odot$ black hole or neutron star accretor, respectively (see also Pearlman et al. 2023). This is consistent with the mass transfer rate required to power bursts from FRB 20200120E with a relatively fainter typical burst luminosity of $L_{FRB} \sim 10^{37}$ erg s^{-1}. We note that FRB 20200120E's localization to a globular cluster furthermore supports a connection with an old progenitor system such as accreting X-ray binaries (Kirsten et al. 2022). Conversely, the deep limit for FRB 20180916B ($L_X \lesssim 8 \times 10^{39}$ erg s^{-1}; Scholz et al. 2020) corresponds to $\sim$5–50 L_{Edd} (Sridhar et al. 2021). We

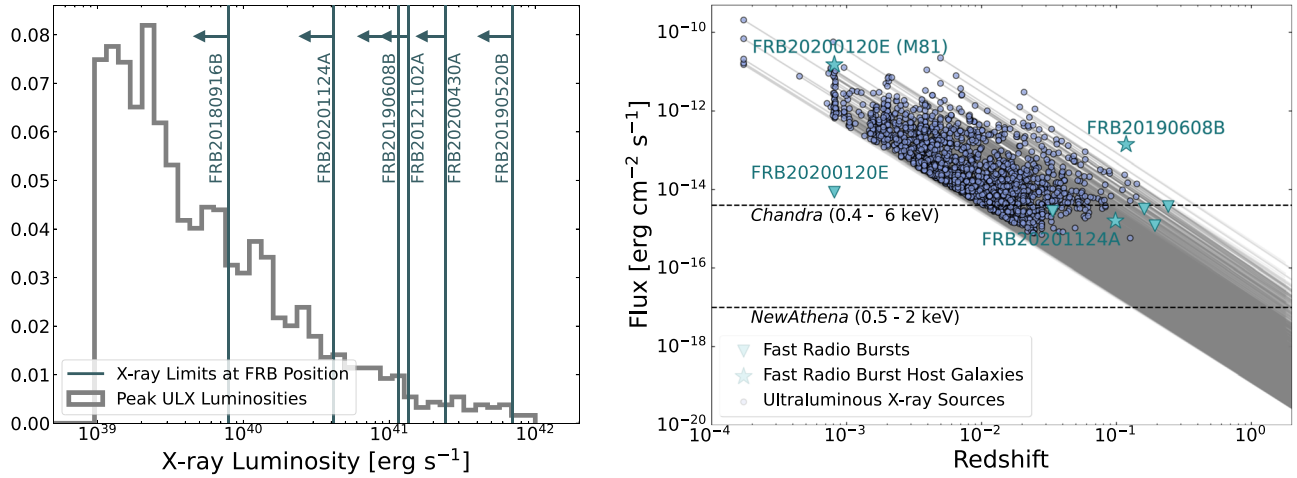

Figure 4. Left: upper limits on the X-ray luminosities of the FRBs in our sample (vertical lines) compared to the luminosity distribution of ULXs from Walton et al. (2022). Not shown is FRB 20200120E, for which the X-ray luminosity limit is $L_X \lesssim 1.3 \times 10^{37}$ erg s^{-1}. Right: X-ray limits (triangles) and detections (stars) for FRBs and FRB hosts respectively, as a function of their redshift. Shown for comparison are the fluxes of ULXs (circles), where gray lines illustrate the flux scaling with redshift. The horizontal dashed lines correspond to the sensitivity of Chandra and the planned NewAthena X-ray observatory. While existing X-ray facilities are sensitive to ULX emission below $z \sim 0.1$, next-generation X-ray observatories such as NewAthena will enable searches for ULX-like counterparts from FRBs out to $z \sim 1$.

note that the X-ray luminosity of the host of FRB 20190608B, which is due to a Type I AGN, is well above the ULX luminosity function as expected.

Future prospects for probing the peak of the ULX luminosity function at $L_X \lesssim 10^{40}$ erg s^{-1} will be aided by the the wealth of low-DM FRBs expected to be discovered and localized by a number of existing and planned FRB facilities (including planned upgrades). In Figure 4 (right panel), we plot the X-ray fluxes of known ULXs (Walton et al. 2022) as a function of their redshift against X-ray fluxes and limits for well-localized FRBs and their hosts. Indeed, while the present-day sample of FRB hosts is dominated by sources at $z \gtrsim 0.1$, well above the population of ULXs, a number of FRB experiments promise to enhance the detection rate of precisely localized low-DM events, pushing into the low-redshift regime where ULXs are primarily detected. Such experiments (and upgrades) include ASKAP with its Commensal Real-time ASKAP Fast Transients Survey (CRAFT; Macquart et al. 2010) COherent upgrade (CRACO) system, the More TRAnsients and Pulsars (MeerTRAP; Sanidas et al. 2018) project on the MeerKAT telescope, and the Deep Synoptic Array (DSA-2000; Connor & Ravi 2023), which will also increase the detection horizon for FRBs out to $z \sim 5$. The large field of view afforded by experiments like the Bustling Universe Radio Survey Telescope in Taiwan (BURSTT; Lin et al. 2022) and the Canadian Hydrogen Intensity Mapping FRB Experiment (CHIME/FRB; CHIME/FRB Collaboration et al. 2018), which will achieve subarcsecond localizations of FRBs beginning in early 2024 thanks to the addition of outrigger telescopes to the array, will significantly increase the rate of well-localized low-DM events. Above $z \gtrsim 0.1$, where the typical ULX flux scaling drops below the Chandra sensitivity threshold (see Figure 4), and as FRB experiments increase their horizon beyond the current $z \sim 1$ (Ryder et al. 2023), it will be possible with next-generation X-ray observatories, such as NewAthena and the Advanced X-ray Imaging Satellite (AXIS), to perform productive searches for ULX-like counterparts.

4.2. Searching for Coincident ULX–FRB Pairs

Taking advantage of the latest ULX catalogs and the hundreds of known FRBs (albeit localized to tens of arcminutes), we search for ULXs coincident with FRBs using the multimission catalog of ULXs (Walton et al. 2022) described in Section 4.1 and the CHIME/FRB catalog (CHIME/FRB Collaboration et al. 2021).[34] The CHIME/FRB catalog includes 536 unique FRBs detected between 2018 July 25 to 2019 July 1. Among this sample, 62 events represent bursts from 18 previously reported repeating FRBs.

We first search for ULXs within 3° of a CHIME/FRB position using the FRB coordinates derived from the metadata headers (CHIME/FRB Collaboration et al. 2021). Given the non-Gaussian nature of the CHIME/FRB localization regions, we do not adopt the positional uncertainties provided in the metadata headers, and instead conservatively impose a $3\sigma = 3°$ localization uncertainty to account for the full extent of the CHIME localization regions. Our initial search returns 641 matches corresponding to 184 unique FRBs. We next manually check whether the matched ULXs actually lie within the FRB localization regions for each event using the HDF5 localization files. After applying this filter, we find a total of 28 ULXs spatially coincident with the localization regions for 17 FRBs. Interestingly, this includes one repeating FRB: FRB20190116A.

To assess whether the remaining FRB–ULX pairs are plausibly related, we plot the redshifts inferred from their DMs for the FRBs as a function of the ULX redshifts (Walton et al. 2022) in Figure 5. We estimate the FRB redshifts using the Macquart relation (Macquart et al. 2020) and two different values of $\mathrm{DM_{host}}$: 0 pc cm^{-3} (shown in light blue on Figure 5) and 150 pc cm^{-3} (dark blue in Figure 5).[35] For the FRB DMs, we adopt the `dm_exc_ne2001` values from the CHIME/FRB catalog, which account for the $\mathrm{DM_{MW}}$ contribution assuming the `NE2001` electron density model (Cordes & Lazio 2002).

[34] https://www.chime-frb.ca/catalog

[35] This is comparable to the median value of $\mathrm{DM_{host}} = 186^{+59}_{-48}$ estimated in James et al. (2022).

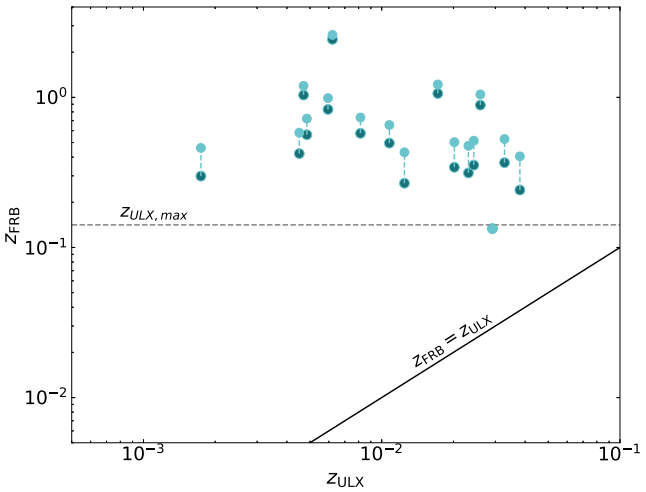

Figure 5. Inferred redshifts for the CHIME/FRB Catalog 1 FRBs ($z_{\rm FRB}$) with coincident ULXs in their localization regions as a function of the ULX redshifts ($z_{\rm ULX}$). Dashed lines connect points with no $\rm DM_{host}$ contribution (light blue) to points with an assumed $\rm DM_{host} = 150\ pc\ cm^{-3}$ (dark blue). The solid diagonal line indicates where $z_{\rm FRB} = z_{\rm ULX}$. The horizontal dashed line at $z \approx 0.14$ corresponds to the maximum observed redshift for a ULX from the complete ULX catalog.

Given the low volumetric distance probed by the existing ULX catalogs, we find that the inferred redshifts for the FRBs in our cross-matched sample are inconsistent with the ULX redshifts, assuming that the true value of $\rm DM_{host}$ lies in the range 0–150 $\rm pc\ cm^{-3}$ and ignoring the scatter in the Macquart relation which may also impact our results (Baptista et al. 2023; James et al. 2022; James 2023; Simha et al. 2023). In particular, inhomogeneities in the baryon distribution of the CGM may bias a DM-inferred redshift lower or higher depending on the cosmic structure along an intervening sightline. We nevertheless conclude that an association between these particular ULX–FRB pairs is unlikely.

5. Conclusions

We have presented the first search for X-ray emission from a sample of FRB host galaxies. Our new Chandra observations, coupled with archival Chandra data, were used to conduct the deepest search for AGN and X-ray counterparts local to seven FRB sources. We also present an updated BPT analysis for 24 highly secure FRB hosts, presenting the nebular line properties for a large sample of FRB host galaxies for the first time. Our key results are summarized as follows.

1. Among the existing sample of seven well-localized FRBs with deep Chandra observations, we find that two of the host galaxies possess nuclear X-ray sources where the emission is powered by a central AGN, including the host of FRB 20200120E (M81), which hosts a known LLAGN. This corresponds to an AGN occupation fraction of ∼20% and ∼50% for repeating and nonrepeating FRBs, respectively, which may point to an elevated rate of AGN in FRB hosts (when compared to field galaxies at similar redshifts). However, these results are based on a small sample size—and uncharacterized selection effects—warranting X-ray observations of a larger sample of hosts.
2. Our detection of luminous ($L_X \approx 5 \times 10^{42}$ erg $\rm s^{-1}$) X-ray emission spatially coincident with the nucleus of the host of FRB 20190608B is consistent with its classification as a Type I Seyfert galaxy, and as such, is the only FRB host known to harbor a Type I AGN. We infer an SMBH mass of $M_{\rm BH} \sim 10^8\,M_\odot$ and an Eddington ratio $L_{\rm bol}/L_{\rm Edd} \approx 0.02$, characteristic of geometrically thin disks in Seyfert galaxies which are less efficient at jet production. We do not detect X-ray emission at the FRB position (offset by $\sim 1\farcs6$ from the host center) and place a limit on the X-ray luminosity at the FRB location of $L_X \lesssim 10^{41}$ erg $\rm s^{-1}$.
3. X-ray limits for the remainder of FRBs in our sample allow us to rule out AGN with $L_X \lesssim 10^{41}$–10^{42} erg $\rm s^{-1}$, including some LLAGN. However, the majority of radio limits for these sources do not reach the regime of radio-quiet AGN.
4. Our updated BPT analysis of 24 FRB hosts demonstrates that FRB host galaxies trace the full underlying galaxy population but are dominated by star-forming galaxies which are largely aligned with the main star-forming locus. We find that the hosts of repeating FRBs are not located exclusively in the star-forming region, however, contrary to previous studies. Similar to earlier findings, we do find evidence for an elevated fraction of hosts occurring in the LINER region.
5. We demonstrate that existing X-ray limits for FRBs are sufficient for probing the bright end of the ULX luminosity function ($L_X \gtrsim 10^{40}$ erg $\rm s^{-1}$), but that the typical redshifts of FRB hosts ($z \gtrsim 0.1$) compared to the local Universe distances of ULXs renders detections at the peak of the luminosity function ($L_X \lesssim 10^{40}$) challenging. Upcoming X-ray observatories like NewAthena and AXIS will extend the detection horizon for ULX-like counterparts to FRBs out to $z \sim 1$. At the same time, upgrades to a number of FRB experiments will lend to an increased rate of low-DM FRBs which will be prime candidates for searching for ULXs at the peak of the ULX luminosity function.
6. Performing a cross-matching analysis between the CHIME/FRB catalog and the largest catalog of ULX sources compiled to date, we find a total of 28 ULXs spatially coincident with the localization regions for 17 FRBs. However, the DM-inferred redshifts for these FRBs imply distances ∼10–10^3 times larger than the distances to the ULXs, and hence we consider any associations unlikely.

Continued X-ray observations of FRB host galaxies will critically probe the occupation fraction of AGN. Understanding the AGN fraction in FRB host galaxies, as well as pinpointing the dominant source of ionizing radiation prevalent in hosts that are optically classified as LINERS, will provide new insight into the stellar populations that should ultimately drive FRB production. Searches for X-ray counterparts will benefit most from dedicated follow up of the most nearby events, where such observations can be most constraining.

Acknowledgments

We thank Kari A. Frank, Paul Green, Alice P. Curtin, Kristina Nyland, and Victoria Kaspi for helpful discussions. T.E. is supported by NASA through the NASA Hubble Fellowship grant HST-HF2-51504.001-A awarded by the Space Telescope Science Institute, which is operated by the

Association of Universities for Research in Astronomy, Inc., for NASA, under contract NAS5-26555. W.F. gratefully acknowledges support by the National Science Foundation under CAREER grant No. AST-2047919, the David and Lucile Packard Foundation, the Alfred P. Sloan Foundation, and the Research Corporation for Science Advancement through Cottrell Scholar Award #28284. N.S. acknowledges the support from NASA (grant No. 80NSSC22K0332), NASA FINESST (grant No. 80NSSC22K1597), and Columbia University Dean's fellowship. S.B. is supported by a Dutch Research Council (NWO) Veni Fellowship (VI.Veni.212.058). Y.D. is supported by the National Science Foundation Graduate Research Fellowship under grant No. DGE-1842165. A.T.D. and R.M.S. acknowledge support through Australian Research Council ARC DP DP220102305. R.M.S. acknowledges support through Australian Research Council Future Fellowship FT190100155. J.X.P., A.C.G., Y.D., W.F., T.E., N.T., and C.D.K. acknowledge support from NSF grants AST-1911140, AST-1910471, and AST-2206490 as members of the Fast and Fortunate for FRB Follow-up team. A.B.P. is a Banting Fellow, a McGill Space Institute (MSI) Fellow, and a Fonds de Recherche du Quebec—Nature et Technologies (FRQNT) postdoctoral fellow.

Facilities: the VLA observations presented here were obtained as part of programs VLA/20A-157, PI: Bhandari and VLA/22B-115, PI: Eftekhari. The VLA is operated by the National Radio Astronomy Observatory, a facility of the National Science Foundation operated under cooperative agreement by Associated Universities, Inc. The Chandra ACIS data for FRB20200120E used in this paper can be found in the Chandra Data Archive under the following Observation IDs for (1) the FRB position: 9540, PI: Jenkins; 4752, PI: Miller; 13728 and 14471, PI: Grise; 18051, 18052, 18817, 19685, 19992 and 19993, PI: Swartz; and (2) the host center: 735, 18047, 18048, 18049, 18050, 18051, 18052, 18053, 18054, 18817, 18875, 19685, 19688, 19981, 19982, 19991, 19992 and 19993, PI: Swartz; 5600, 5601, 6174, 6346, and 6347, PI: Canizares; 5935, 5936, 5937, 5938, 5939, 5940, 5941, 5942, 5943, 5944, 5945, 5946, 5947, 5948 and 5949, PI: Pooley; 4752, 6892, 6893, 6894, 6895, 6896, 6897, 6898, 6899, 6900 and 6901, PI: Miller; 9122, PI: Immler; 9540, 9805, PI: Jonker; 12301, PI: Dwarkadas; 13728, 14471, PI: Grise; 20624, PI: Barth; 21384, PI: Irwin; 26421, PI: Brightman.

Software: `astropy` (Astropy Collaboration et al. 2022), `CASA` (McMullin et al. 2007), `CIAO` (v4.13) (Fruscione et al. 2006), `matplotlib` (Hunter 2007), `numpy` (Harris et al. 2020), `pandas` (Reback 2022), `Prospector` (Johnson et al. 2021), `SAOImageDS9` (Joye & Mandel 2003), `SExtractor` (Bertin & Arnouts 1996), `scipy` (Virtanen et al. 2020), `superchandra` (Kilpatrick 2023), and `xspec` (Arnaud 1996).

ORCID iDs

T. Eftekhari https://orcid.org/0000-0003-0307-9984
W. Fong https://orcid.org/0000-0002-7374-935X
A. C. Gordon https://orcid.org/0000-0002-5025-4645
N. Sridhar https://orcid.org/0000-0002-5519-9550
C. D. Kilpatrick https://orcid.org/0000-0002-5740-7747
S. Bhandari https://orcid.org/0000-0003-3460-506X
A. T. Deller https://orcid.org/0000-0001-9434-3837
Y. Dong (董雨 欣) https://orcid.org/0000-0002-9363-8606
A. Rouco Escorial https://orcid.org/0000-0003-3937-0618
K. E. Heintz https://orcid.org/0000-0002-9389-7413
J. Leja https://orcid.org/0000-0001-6755-1315
B. Margalit https://orcid.org/0000-0001-8405-2649
B. D. Metzger https://orcid.org/0000-0002-4670-7509
A. B. Pearlman https://orcid.org/0000-0002-8912-0732
J. X. Prochaska https://orcid.org/0000-0002-7738-6875
S. D. Ryder https://orcid.org/0000-0003-4501-8100
P. Scholz https://orcid.org/0000-0002-7374-7119
R. M. Shannon https://orcid.org/0000-0002-7285-6348
N. Tejos https://orcid.org/0000-0002-1883-4252

References

Abramowicz, M. A., Bejger, M., & Wielgus, M. 2018, ApJ, 868, 17
Aggarwal, K., Budavári, T., Deller, A. T., et al. 2021, ApJ, 911, 95
Arnaud, K. A. 1996, in ASP Conf. Ser. 101, Astronomical Data Analysis Software and Systems V, ed. G. H. Jacoby & J. Barnes (San Francisco, CA: ASP), 17
Asplund, M., Grevesse, N., Sauval, A. J., & Scott, P. 2009, ARA&A, 47, 481
Astropy Collaboration, Price-Whelan, A. M., & Lim, P. L. 2022, ApJ, 935, 167
Baldwin, J. A., Phillips, M. M., & Terlevich, R. 1981, PASP, 93, 5
Ballo, L., Heras, F. J. H., Barcons, X., & Carrera, F. J. 2012, A&A, 545, A66
Balmaverde, B., & Capetti, A. 2006, A&A, 447, 97
Baptista, J., Prochaska, J. X., Mannings, A. G., et al. 2023, Measuring the Variance of the Macquart Relation in z-DM Modeling arXiv:2305.07022
Bertin, E., & Arnouts, S. 1996, A&AS, 117, 393
Bhandari, S., Gordon, A. C., Scott, D. R., et al. 2023, ApJ, 948, 67
Bhandari, S., Heintz, K. E., Aggarwal, K., et al. 2022, AJ, 163, 69
Bhandari, S., Sadler, E. M., Prochaska, J. X., et al. 2020, ApJL, 895, L37
Bhardwaj, M., Kirichenko, A. Y., Michilli, D., et al. 2021, ApJL, 919, L24
Bochenek, C. D., Ravi, V., Belov, K. V., et al. 2020, Natur, 587, 59
Brusa, M., Zamorani, G., Comastri, A., et al. 2007, ApJS, 172, 353
Cantiello, M., Jermyn, A. S., & Lin, D. N. C. 2021, ApJ, 910, 94
Cash, W. 1979, ApJ, 228, 939
Chatterjee, S., Law, C. J., Wharton, R. S., et al. 2017, Natur, 541, 58
Chiaberge, M., Capetti, A., & Macchetto, F. D. 2005, ApJ, 625, 716
CHIME/FRB Collaboration, Amiri, M., Andersen, B. C., et al. 2020, Natur, 582, 351
CHIME/FRB Collaboration, Amiri, M., & Andersen, B. C. 2021, ApJS, 257, 59
CHIME/FRB Collaboration, Amiri, M., Bandura, K., et al. 2018, ApJ, 863, 48
CHIME/FRB Collaboration, Anderson, B. C., Bandura, K., et al. 2023, ApJ, 947, 83
CHIME/FRB Collaboration, Andersen, B. C., Bandura, K. M., et al. 2020, Natur, 587, 54
Chittidi, J. S., Simha, S., Mannings, A., et al. 2021, ApJ, 922, 173
Cid Fernandes, R., Stasińska, G., Schlickmann, M. S., et al. 2010, MNRAS, 403, 1036
Connor, L., & Ravi, V. 2023, MNRAS, 521, 4024
Cordes, J. M., & Lazio, T. J. W. 2002, arXiv:astro-ph/0207156
Cornwell, T. J., Golap, K., & Bhatnagar, S. 2008, ISTSP, 2, 647
Costa, R., Gordin, J. E. B., & Weltman, A. 2018, arXiv:1807.01976
Cramér, H. 1928, Scand Actuar J, 1928, 13
Day, C. K., Deller, A. T., James, C. W., et al. 2021, PASA, 38, e050
Deng, C. M., Zhong, S. Q., & Dai, Z. G. 2021, ApJ, 922, 98
Dey, A., Schlegel, D. J., Lang, D., et al. 2019, AJ, 157, 168
Dudik, R. P., Satyapal, S., Gliozzi, M., & Sambruna, R. M. 2005, ApJ, 620, 113
Eftekhari, T., & Berger, E. 2017, ApJ, 849, 162
Fruscione, A., McDowell, J. C., Allen, G. E., et al. 2006, Proc. SPIE, 6270, 62701V
Garg, P., Narayanan, D., Byler, N., et al. 2022, ApJ, 926, 80
Gehrels, N. 1986, ApJ, 303, 336
Gordon, A. C., Fong, W.-f., Kilpatrick, C. D., et al. 2023, ApJ, 954, 80
Greiner, J., Michałowski, M. J., Klose, S., et al. 2016, A&A, 593, A17
Gross, A. C., Fu, H., Myers, A. D., Wrobel, J. M., & Djorgovski, S. G. 2019, ApJ, 883, 50
Güver, T., & Özel, F. 2009, MNRAS, 400, 2050
Harris, C. R., Millman, K. J., van der Walt, S. J., et al. 2020, Natur, 585, 357
Heckman, T. M. 1980, A&A, 87, 152
Heintz, K. E., Prochaska, J. X., Simha, S., et al. 2020, ApJ, 903, 152
Ho, L. C. 2008, ARA&A, 46, 475
Ho, L. C., Feigelson, E. D., Townsley, L. K., et al. 2001, ApJL, 549, L51
Ho, L. C., Filippenko, A. V., & Sargent, W. L. W. 1996, ApJ, 462, 183

Ho, L. C., & Peng, C. Y. 2001, ApJ, 555, 650
Hunter, J. D. 2007, CSE, 9, 90
Ibik, A. L., Drout, M. R., Gaensler, B. M., et al. 2023, arXiv:2304.02638
James, C. W. 2023, PASA, in press (arXiv:2306.17403)
James, C. W., Ghosh, E. M., Prochaska, J. X., et al. 2022, MNRAS, 516, 4862
Jermyn, A. S., Dittmann, A. J., Cantiello, M., & Perna, R. 2021, ApJ, 914, 105
Johnson, B. D., Leja, J., Conroy, C., & Speagle, J. S. 2021, ApJS, 254, 22
Joye, W. A., & Mandel, E. 2003, in ASP Conf. Ser. 295, Astronomical Data Analysis Software and Systems XII, ed. H. E. Payne, R. I. Jedrzejewski, & R. N. Hook (San Francisco, CA: ASP), 489
Kauffmann, G., Heckman, T. M., Tremonti, C., et al. 2003, MNRAS, 346, 1055
Kellermann, K. I., Sramek, R., Schmidt, M., Shaffer, D. B., & Green, R. 1989, AJ, 98, 1195
Kilpatrick, C. D. 2023, charliekilpatrick/superchandra: superchandra v1.0.1, Zenodo, doi:10.5281/zenodo.8111021
Kirsten, F., Marcote, B., Nimmo, K., et al. 2022, Natur, 602, 585
Kormendy, J., & Ho, L. C. 2013, ARA&A, 51, 511
Kumari, N., Maiolino, R., Trussler, J., et al. 2021, A&A, 656, A140
LaMassa, S. M., Urry, C. M., Cappelluti, N., et al. 2016, ApJ, 817, 172
Law, C. J., Sharma, K., Ravi, V., et al. 2023, arXiv:2307.03344
Lin, H. H., Lin, K. y., Li, C. T., et al. 2022, PASP, 134, 094106
Lorimer, D. R., Bailes, M., McLaughlin, M. A., Narkevic, D. J., & Crawford, F. 2007, Sci, 318, 777
Macquart, J. P., Bailes, M., Bhat, N. D. R., et al. 2010, PASA, 27, 272
Macquart, J. P., Prochaska, J. X., McQuinn, M., et al. 2020, Natur, 581, 391
Marcote, B., Nimmo, K., Hessels, J. W. T., et al. 2020, Natur, 577, 190
Margalit, B., Beniamini, P., Sridhar, N., & Metzger, B. D. 2020, ApJL, 899, L27
Margalit, B., Berger, E., & Metzger, B. D. 2019, ApJ, 886, 110
Margalit, B., & Metzger, B. D. 2018, ApJL, 868, L4
Martini, P., Sivakoff, G. R., & Mulchaey, J. S. 2009, ApJ, 701, 66
Martín-Navarro, I., Brodie, J. P., Romanowsky, A. J., Ruiz-Lara, T., & van de Ven, G. 2018, Natur, 553, 307
McMullin, J. P., Waters, B., Schiebel, D., Young, W., & Golap, K. 2007, in ASP Conf. Ser. 376, Astronomical Data Analysis Software and Systems XVI, ed. R. A. Shaw, F. Hill, & D. J. Bell (San Francisco, CA: ASP), 127
Middleton, M. J., Fragile, P. C., Ingram, A., & Roberts, T. P. 2019, MNRAS, 489, 282
Miller, J. M., Nowak, M., Markoff, S., Rupen, M. P., & Maitra, D. 2010, ApJ, 720, 1033
Mises, R. V. 1928, ZAMM, 8, 161
Murphy, E. J., Condon, J. J., Schinnerer, E., et al. 2011, ApJ, 737, 67
Niu, C. H, Aggarwal, K, & Li, D 2022, Natur, 606, 873
Panessa, F., Baldi, R. D., Laor, A., et al. 2019, NatAs, 3, 387
Panessa, F., Barcons, X., Bassani, L., et al. 2007, A&A, 467, 519
Pearlman, A. B., Scholz, P., Bethapudi, S., et al. 2023, arXiv:2308.10930
Pelliciari, D., Bernardi, G., Pilia, M., et al. 2023, A&A, 674, A223
Perna, R., Lazzati, D., & Cantiello, M. 2021a, ApJL, 906, L7
Perna, R., Tagawa, H., Haiman, Z., & Bartos, I. 2021b, ApJ, 915, 10
Piconcelli, E., Jimenez-Bailón, E., Guainazzi, M., et al. 2005, A&A, 432, 15
Piro, L., Bruni, G., Troja, E., et al. 2021, A&A, 656, L15
Planck Collaboration, Aghanim, N., & Akrami, N. 2020, A&A, 641, A6
Pleunis, Z., Good, D. C., Kaspi, V. M., et al. 2021, ApJ, 923, 1
Rajwade, K. M., Mickaliger, M. B., Stappers, B. W., et al. 2020, MNRAS, 495, 3551
Ravi, V., Catha, M., Chen, G., et al. 2023, ApJL, 949, L3
Ravi, V., Law, C. J., Li, D., et al. 2022, MNRAS, 513, 982
Reback, J., 2022 pandas-dev/pandas: Pandas 1.4.2, v1.4.2, Zenodo, doi:10.5281/zenodo.6408044
Reines, A. E., Condon, J. J., Darling, J., & Greene, J. E. 2020, ApJ, 888, 36
Reines, A. E., & Volonteri, M. 2015, ApJ, 813, 82
Ryder, S. D., Bannister, K. W., Bhandari, S., et al. 2023, Sci, 382, 294
Sanidas, S., Caleb, M., Driessen, L., et al. 2018, in IAU Symp. 337, Pulsar Astrophysics the Next Fifty Years, ed. P. Weltevrede (Cambridge: Cambridge Univ. Press), 406
Satyapal, S., Sambruna, R. M., & Dudik, R. P. 2004, A&A, 414, 825
Sault, R. J., & Wieringa, M. H. 1994, A&AS, 108, 585
Schlafly, E. F., & Finkbeiner, D. P. 2011, ApJ, 737, 103
Scholz, P., Bogdanov, S., Hessels, J. W. T., et al. 2017, ApJ, 846, 80
Scholz, P., Cook, A., Cruces, M., et al. 2020, ApJ, 901, 165
Scholz, P., Spitler, L. G., Hessels, J. W. T., et al. 2016, ApJ, 833, 177
Shannon, R. M., Macquart, J. P., Bannister, K. W., et al. 2018, Natur, 562, 386
Sharma, K., Somalwar, J., Law, C., et al. 2023, ApJ, 950, 175
She, R., Ho, L. C., & Feng, H. 2017, ApJ, 842, 131
Simha, S., Lee, K. G., Prochaska, J. X., et al. 2023, ApJ, 954, 71
Singh, R., van de Ven, G., Jahnke, K., et al. 2013, A&A, 558, A43
Spitler, L. G., Scholz, P., Hessels, J. W. T., et al. 2016, Natur, 531, 202
Sridhar, N., Metzger, B. D., Beniamini, P., et al. 2021, ApJ, 917, 13
Sridhar, N., Metzger, B. D., & Fang, K. 2022, arXiv:2212.11236
Sridhar, N., Zrake, J., Metzger, B. D., Sironi, L., & Giannios, D. 2021, MNRAS, 501, 3184
Stern, J., & Laor, A. 2012, MNRAS, 426, 2703
Terashima, Y., & Wilson, A. S. 2003, ApJ, 583, 145
Thornton, D., Stappers, B., Bailes, M., et al. 2013, Sci, 341, 53
Virtanen, P., Gommers, R., Oliphant, T. E., et al. 2020, NatMe, 17, 261
Walton, D. J., Mackenzie, A. D. A., Gully, H., et al. 2022, MNRAS, 509, 1587
Waxman, E. 2017, ApJ, 842, 34
Willingale, R., Starling, R. L. C., Beardmore, A. P., Tanvir, N. R., & O'Brien, P. T. 2013, MNRAS, 431, 394
Xu, Y. D., & Cao, X. W. 2009, RAA, 9, 401
Yun, M. S., & Carilli, C. L. 2002, ApJ, 568, 88
Zhang, B. 2017, ApJL, 836, L32
Zubovas, K., & King, A. R. 2012, MNRAS, 426, 2751